An Ab Initio, Fully Coherent, Semi-Analytical Model of Surface-Roughness-Induced Scattering

Samuel M. Hörmann, Jakob W. Hinum-Wagner, and Alexander Bergmann

***Abstract*—Integrated optics and silicon photonics is a rapidly maturing technology and is progressing in telecom, computation, and sensing. Surface-roughness-induced scattering is the primary source of optical loss in most photonic integrated circuits, and as such, ultimately limits the performance of their applications. However, a closed-form description for arbitrary refractive index profiles remains lacking, even though such a one is essential to enable an objective-oriented design of the waveguide platform. We present an ab initio, fully coherent, analytical model based on the volume current method that uses the surface roughness' autocorrelation function and the unperturbed mode's electromagnetic fields to predict the loss coefficient in closed form. An improved expression for the perturbation facilitates the application also to high-index-contrast systems. Hence, it is flexible concerning wavelength, materials, fabrication process, geometry and mode. Consequently, our model may be seamlessly integrated into electromagnetic simulation software suites, once the surface roughness is known for the utilized fabrication process. To verify our model, we compare the calculated scattering losses to measured propagation losses and established models for a wide range of waveguide systems in literature. We find that the previously neglected correlation along the waveguide height significantly impacts the scattering, which necessitates the holistic statistical analysis of the surface roughness. We believe these comprehensive prediction capabilities to be a useful tool for the optimization of silicon photonics design and fabrication, especially for low-confinement applications like sensors.**

***Index Terms*—Integrated optics, optical loss, optical scattering, photonic integrated circuits, silicon photonics, surface roughness.**

I. Introduction

INTEGRATED photonics unlocks light for the transport of information and sensing applications on top of a substrate. Silicon photonics is the prevalent technology since it enables seamless fabrication in electronics foundries [1], [2].

Manuscript received 27 September 2022; revised 15 November 2022; accepted 22 November 2022. Date of publication 25 November 2022; date of current version 3 March 2023. *(Corresponding author: Samuel M. Hörmann.)*

Samuel M. Hörmann is with the Institute of Electrical Measurement and Sensor Systems, Graz University of Technology, 8010 Graz, Austria, and also with the ams-OSRAM AG, 8141 Unterpremstätten, Austria (e-mail: samuel.hoermann@student.tugraz.at).

Jakob W. Hinum-Wagner is with the Institute of Electrical Measurement and Sensor Systems, Graz University of Technology, 8010 Graz, Austria, and also with the ams-OSRAM AG, 8141 Unterpremstätten, Austria (e-mail: j.hinum-wagner@tugraz.at).

Alexander Bergmann is with the Institute of Electrical Measurement and Sensor Systems, Graz University of Technology, 8010 Graz, Austria (e-mail: alexander.bergmann@tugraz.at).

Color versions of one or more figures in this article are available at https://doi.org/10.1109/JLT.2022.3224777.

Digital Object Identifier 10.1109/JLT.2022.3224777

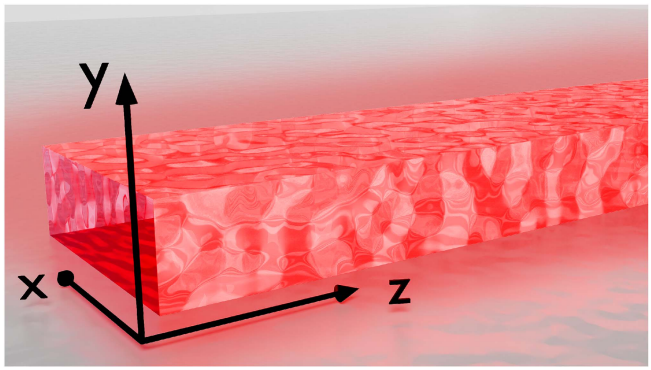

Fig. 1. Stylized surface-roughness-induced scattering losses in a strip waveguide atop a substrate.

Conceptually, integrated photonics relies on waveguides that confine guided modes. From a platform design perspective, the propagation loss coefficient is essential in finding a balance between performance and footprint [3]. On the device level, the applications are ultimately limited in performance and characterized thereby, e.g., setting the intrinsic Q-factor of resonator structures [1]. Thus, it has a central, fundamental impact on the limit of detection (LOD) of integrated photonic sensors [2], [4]. Further, ultra-high Q-factor resonators are also attractive for integrated photonic filters, delay lines, and modulators [5], [6]. Hence, a model to describe the loss occurring in waveguides is necessary for the objective-driven design of any integrated photonic device.

A. Loss in Waveguides

Losses in waveguides can be described by three main components: First, absorption is caused by the waveguide material. Secondly, the number of bound modes is finite, and a continuum of radiative modes exists. Surface roughness, as depicted in Fig. 1, acts as a perturbation and couples the guided and radiative modes. And thirdly, the surface roughness also scatters into the guided mode in the opposite direction, i.e. with $-\beta$. This backscattering can even be more compromising to the sensor system than a simple power loss because the laser can be disturbed. Typically, the material absorption losses are smaller than the surface-roughness-induced scattering losses and can be neglected [7], [8], [9].

The surface roughness is embodied by imperfections created during the waveguide fabrication, mostly by lithography and etching processes. The commonly used top-down fabrication

concentrates most of the roughness on the sidewalls, as described in detail by Melloni et al. [9]. Previously, it was argued that the sidewall is a series of vertical striations [10], [11], [12]. Even if deviations were observed, the impact on the scattering was assumed to be negligible [9].

A widely used model for the surface-roughness-induced scattering loss was devised by Payne and Lacey [7]. It is an approximation based on the assumption of slab waveguides. It is parametric and specific to a fixed geometry and mode. However, the ab initio design of a waveguide system necessitates more flexible models. Yap et al. [13] introduced a correction factor in the Payne and Lacey model accounting for the electric field strength at the sidewalls. The modified model was applied to Si rib waveguides, but had difficulties in predicting the loss coefficient correctly. One of the reasons might be the inability of a parametric model to account for arbitrary refractive index profiles.

Hughes et al. [14] devised a model for losses occurring in photonic crystals (PhC) that distinguishes between radiative losses α_r and back-scattering α_b, and in which the dependence on the group velocity and the modes' field distributions are considered:

$$\alpha = n_g \alpha_r + n_g^2 \alpha_b \tag{1}$$

where n_g is the effective group index calculated from the effective refractive index as $n_g = n_e - \omega \frac{dn_e}{d\omega}$. This model is also extensively discussed by Melloni et al. [9] and Schulz [15].

A flexible approach is the volume current method (VCM), which includes the surface roughness as a perturbation in the form of an oscillating volume current [10]. The volume current can be viewed as emitting dipoles, whose far field radiation is the scattering loss. This model considers the statistical properties of the surface roughness and is flexible concerning wavelength, materials, fabrication process, and mode. In low-index-contrast waveguides, the situation may be approximated and closed-form solutions may be derived. However, in high-index-contrast waveguides the discontinuity at the waveguide interface demands either an additional approximation depending on the geometry [10] or a FDTD simulation [12], [16], [17]. Moreover, this represents a barrier for the consideration of the surface-roughness-induced scattering losses in electrodynamics simulation suites.

Utilizing the perturbation from Johnson et al. [18], we present an ab initio, semi-analytical model for a guided-wave platform's surface-roughness-induced scattering loss coefficient. In contrast to the established VCM, our modification allows arbitrary refractive index profiles to be computed, including systems with high index contrasts. Due to the closed form, our model can be seamlessly integrated into electrodynamics simulation suites. Furthermore, we found conflicting evidence regarding the common assumption of perfect vertical striations in sidewall roughness measurements [11], [19], [20], [21], and in a previous analysis [16]. Hence, we incorporate the surface roughness as a Gaussian process which enables the fully coherent consideration of the whole surface. We observe a significant dependency of the loss coefficient on the previously neglected degree of anisotropy.

II. Surface-Roughness-Induced Scattering

A. Guided Wave Optics

A waveguide confines the light laterally and its translation invariance in the propagation direction $\hat{\boldsymbol{z}}$ (see Fig. 1) induces modes for the electromagnetic fields of the form

$$\boldsymbol{E}(\boldsymbol{r}, t) = \boldsymbol{e}(x, y) e^{(i\beta - \alpha) z - i\omega t} \tag{2}$$

where $\boldsymbol{E}$ is the electric field, and $\boldsymbol{e}(x, y)$ its amplitude that is constant in z, t. The mode oscillates at the angular frequency ω and travels as defined via the propagation coefficient β and decays with the attenuation coefficient α. Often, the effective refractive index $n_e = \frac{\beta c}{\omega}$ is used alternatively to the propagation coefficient to characterize the mode, where c is the speed of light in vacuum. The magnetic field $\boldsymbol{H}$ can be written analogously. Typically, the time dependency is omitted and the time derivatives in Maxwell's equations are replaced by $-i\omega$.

B. Perturbation

To calculate the effect of any small change in the material parameters of the waveguide system in terms of the unperturbed modes, we employ perturbation theory. To this end, we use the source-less form of Maxwell's equations with loss-less material parameters. The perturbed mode is defined by a perturbation $\epsilon_p(\boldsymbol{r})$ of the permittivity in Ampere's law [10].

$$\nabla \times \boldsymbol{H}(\boldsymbol{r}) = -i\omega \left[\epsilon(x, y) + \epsilon_p(\boldsymbol{r})\right] \boldsymbol{E}(\boldsymbol{r}) \tag{3}$$

For the validity of a perturbative approach, $\epsilon_p(\boldsymbol{r})$ needs to be either small and/or confined to a small cross-sectional area S_p.

C. Roughness Statistics

In this section, we aim to elaborate on how a perturbation due to the surface roughness created by imperfections in the waveguides' fabrication processes can be described. The permittivity perturbation due to an analyte in a biosensor is straightforward in that the permittivity simply changes slightly in value by ϵ_p in a cross-sectional area S_p. However, it is not so trivial when the material boundary between the waveguide and its surrounding medium shifts according to the surface roughness. There were multiple papers devoted to this issue [11], [18], [22], [23]. First, the perturbation due to the shift Δh of a planar interface at $x = x_0$ is formulated in first-order as

$$\epsilon_p(\boldsymbol{r}) = \frac{\partial \epsilon}{\partial h}(\boldsymbol{r}) \Delta h(\boldsymbol{r}) = (\epsilon_w - \epsilon_s) \delta(x - x_0) \Delta h(y, z) \tag{4}$$

where ϵ_w and ϵ_s are the permittivities of the waveguide and the surrounding medium, respectively. Secondly, the tangential and perpendicular components of the field vectors w.r.t. the interface are distinguished to conform to the interface boundary conditions [18]. Thus, an improved expression for the permittivity

perturbation is found by

$$\epsilon_p(\boldsymbol{r})\boldsymbol{e}(x,y) = \begin{pmatrix} \frac{\Delta\epsilon}{\epsilon_w\epsilon_s}\epsilon^2(x,y)\, e_x(x,y) \\ \Delta\epsilon\, e_y(x,y) \\ \Delta\epsilon\, e_z(x,y) \end{pmatrix} \Delta h(y,z)\delta(x-x_0) \tag{5}$$

with the permittivity difference between the waveguide and its environment $\Delta\epsilon = \epsilon_w - \epsilon_s$.

It is commonly accepted that the sidewall roughness is the main contributor to the scattering losses [7], [8], [9]. For simplicity, we restrict our observation to a single sidewall surface. Hence, the perturbation is a function of (y,z). $\Delta h(y,z)$ can be statistically described by a Gaussian process $H_G(y,z)$ where G is a random variable with sample space Ω_G and probability distribution p_G [24]. The sidewall roughness of a particular waveguide is a sample function thereof, i.e. $H_g(y,z) = \Delta h(y,z,g)$, where g is a realization of G. In general, we denote the expectation value of a stochastic process with

$$\mathbb{E}\left(H_G(y,z)\right) := \int_{\Omega_G} H_g(y,z)p_G(g)dg \tag{6}$$

A zero-mean Gaussian process is completely described by its autocorrelation function, the kernel

$$\kappa(\Delta y,\Delta z) = \mathbb{E}\left(H_G(y,z)H_G(y+\Delta y,z+\Delta z)\right) \tag{7}$$

In our case, the process is stationary, which implies that its kernel depends only on the distance of the arguments. Essentially, the kernel defines the similarity of two neighboring function values. For a separable, multi-dimensional domain, we can decompose the Gaussian process into its subspaces

$$H_G(y,z) = H_Y(y)H_Z(z) \tag{8}$$

with the independent random variables Y and Z. Analogously, the kernel factors into

$$\kappa(\Delta y,\Delta z) = \kappa_y(\Delta y)\kappa_z(\Delta z) \tag{9}$$

The 1D-process, which appropriately models the surface roughness of waveguides, was found to be an Ornstein-Uhlenbeck process with its exponential kernel [9]

$$\kappa_z(\Delta z) = \sigma^2 e^{-\frac{1}{L_c}|\Delta z|} \tag{10}$$

with the RMS-roughness σ and the correlation length L_c. To facilitate the correct dimensions in the multi-dimensional process (9), we formulate

$$\kappa(\Delta y,\Delta z) = \sigma^2 e^{-\frac{1}{L_{c,y}}|\Delta y|}e^{-\frac{1}{L_{c,z}}|\Delta z|} \tag{11}$$

$$\kappa_y(\Delta y) = e^{-\frac{1}{L_{c,y}}|\Delta y|} \tag{12}$$

where we shift σ^2 completely to κ_z for unambiguity and simplicity.

Previously, the sidewall roughness was considered as a series of vertical striations at the waveguide sidewalls [9], [10], [12], which was supported by atomic force microscopy (AFM) measurements, e.g. in [11]. This simpler case corresponds to setting $\kappa_y(\Delta y) \approx 1$ over the waveguide height.

D. Loss Coefficient

We recognize that the perturbation in Ampere's law (3) can be equivalently thought of as an imaginary current $\boldsymbol{J}(\boldsymbol{r}) = -i\omega\epsilon_p(x,y)\boldsymbol{E}_l(\boldsymbol{r})$ in the volume V_p that causes the scattered field. The total field would be a superposition of $\boldsymbol{E}(\boldsymbol{r})$ and the scattered field caused by $\boldsymbol{J}(\boldsymbol{r})$. Concerning the radiation, however, we know that $\boldsymbol{E}(\boldsymbol{r})$ is confined and does not contribute to the losses. Hence, only the scattered field and by extension only $\boldsymbol{J}(\boldsymbol{r})$ need to be considered. We employ a first-order approximation that ignores coupling between the near and the far field radiation. In other words, we integrate the far field radiation intensity directly caused by (3) and assume that this is the power lost to the waveguide system. Following the calculation of the radiation of current distributions by Orfanidis [25], a radiation field may be constructed

$$\boldsymbol{F}(\boldsymbol{k}) = \int_{V_p} d^3r\, \boldsymbol{J}(\boldsymbol{r})e^{-i\boldsymbol{k}\cdot\boldsymbol{r}} \tag{13}$$

where $\boldsymbol{k} = \hat{\boldsymbol{r}}k$. k is the propagation coefficient in the medium in the far field. By setting $k = k_0$ we can transfer the problem into empty space, which later allows us to integrate over the whole solid angle and neglect any refraction. This simpler picture is justified by the preceding first-order approximation, according to which the scattered radiation is not coupled back or absorbed. Notably, we retain the system's correct perturbation from (5). The radiation intensity is deduced from the radiation field's θ- and ϕ-components in spherical coordinates:

$$U(\theta,\phi) = \frac{\mu_0\omega^2}{32\pi^2 c_0}\left[|F_\theta(\theta,\phi)|^2 + |F_\phi(\theta,\phi)|^2\right] \tag{14}$$

This is equivalent to computing the radiation intensity from the magnetic vector potential [10]. Plugging in (3) and (13), and dividing by L to evaluate the radiated intensity per waveguide length, we obtain the specific radiation intensity

$$u(\theta,\phi) = \frac{\mu_0\omega^4}{32\pi^2 c_0\, L}\int_{V_p} d^3r \int_{V_p} d^3r' \epsilon_p(\boldsymbol{r})\boldsymbol{E}(\theta,\phi,\boldsymbol{r})\cdot\epsilon_p(\boldsymbol{r}')\boldsymbol{E}^*(\theta,\phi,\boldsymbol{r}')e^{-i\boldsymbol{k}(\boldsymbol{r}-\boldsymbol{r}')} \tag{15}$$

with the transformed field

$$\boldsymbol{E}(\theta,\phi,\boldsymbol{r}) = \hat{R}(\theta,\phi)\boldsymbol{E}(\boldsymbol{r}) \tag{16a}$$

$$\hat{R}(\theta,\phi) = \begin{pmatrix} 0 & 0 & 0 \\ \cos\theta\cos\phi & \cos\theta\sin\phi & -\sin\theta \\ -\sin\phi & \cos\phi & 0 \end{pmatrix} \tag{16b}$$

Using the perturbation in (5), the x-integral will dissolve due to the δ-distribution. With the assumption of a long waveguide w.r.t. the correlation length, the few z-dependent integrands may be collected and their integrals evaluate to the Gaussian process' z-spectrum S_z via the ergodicity- and Wiener-Khinchin-theorem [26]:

$$\frac{1}{L}\int_0^L dz \int_0^L dz' \Delta h(z)\Delta h(z')e^{i(\beta-k_z)(z-z')} = \pi S_z(\beta-k_z) \tag{17}$$

The spectrum of a Gaussian process is defined by the Fourier transform

$$\pi S(q) := \frac{1}{2}\int_{-\infty}^{\infty} d\Delta z\, \kappa(\Delta z) e^{iq\Delta z} \tag{18}$$

and we find for the exponential kernel (10)

$$\pi S_z(q) = \sigma^2 \frac{L_{c,z}}{1+(qL_{c,z})^2} \tag{19}$$

To condense (15) after inserting (17) and (20), we define the overlap

$$o(\theta,\phi,y,y') = \begin{pmatrix} \frac{\Delta\epsilon}{\epsilon_w \epsilon_s}\epsilon^2(x_0,y)\, e_x(x_0,y) \\ \Delta\epsilon\, e_y(x_0,y) \\ \Delta\epsilon\, e_z(x_0,y) \end{pmatrix} \cdot \hat{T}(\theta,\phi) \begin{pmatrix} \frac{\Delta\epsilon}{\epsilon_w \epsilon_s}\epsilon^2(x_0,y')\, e_x^*(x_0,y') \\ \Delta\epsilon\, e_y^*(x_0,y') \\ \Delta\epsilon\, e_z^*(x_0,y') \end{pmatrix} \tag{20}$$

with

$$\hat{T}(\theta,\phi) = \hat{R}^T(\theta,\phi)\hat{R}(\theta,\phi) \tag{21}$$

Eventually, the radiation intensity (15) becomes

$$u(\theta,\phi) = \frac{\mu_0\omega^4}{32\pi^2 c_0}\pi S_z(\beta - k_z)\int_0^H dy \int_0^H dy' \kappa_y(y-y') o(\theta,\phi,y,y') e^{-ik_y(y-y')} \tag{22}$$

where $\Delta h(y)\Delta h(y')$ was transformed into $\kappa_y(y-y')$ by applying the expectation value. The components of $\boldsymbol{k}$ are $k_y = \sin(\theta)\sin(\phi)k$ and $k_z = \cos(\theta)k$. The integrals range over the waveguide height H. The total radiated power per unit length is obtained by integrating (22) over the solid angle. Finally, the loss coefficient may be evaluated

$$2\alpha = \frac{1}{P}\int_0^{\pi} d\theta \sin(\theta)\int_0^{2\pi} d\phi\, u(\theta,\phi) \tag{23}$$

with the input mode power P corresponding to the z-component of the integrated Poynting vector [27]:

$$P = \frac{1}{2}\int_{-\infty}^{\infty} dx \int_{-\infty}^{\infty} dy\, \Re\left[(\boldsymbol{e}\times\boldsymbol{h}^*)\cdot\hat{\boldsymbol{z}}\right] \tag{24}$$

The factor of two in front of α relates the power loss to the attenuation coefficient of the mode's fields from (2).

The expression derived above enables the semi-analytical calculation of explicit values for the loss in a waveguide. The key improvement of our model is to use the perturbation (5) that correctly conforms the scattered fields to the boundary conditions of the material cross section. Furthermore, the only inputs required in (22) are the surface roughness parameters considered via the Gaussian process spectrum and autocorrelation function, and the fields of the unperturbed mode that is under consideration. The latter can be simulated in suitable simulation suites or frameworks. Hence, our calculation of the loss coefficients may be seamlessly integrated into simulations of the unperturbed waveguide system. The extracted field values, or rather, the overlap o may be integrated via common numerical integration routines based on quadrature. For the final calculation of the loss coefficient, the integration over the solid angle can be implemented via adaptive methods to enhance accuracy.

Our model relies on a first-order approximation that ignores coupling between the near and the far field radiation, i.e. we do not consider scattered far field radiation that is coupled back into guided modes, or near field radiation that is scattered into the far field or absorbed. Hence, the scattered far field radiation intensity is assumed immediately lost, and reflection and refraction at the system's material interfaces do not impact the perturbation. This assumption inevitably leads to less accuracy as compared to sophisticated FDTD methods [12], [16], [17], but is expected to improve on simplifications in [10] and [11] for waveguides that are not conformal to their assumed geometries.

Additionally, we assumed $L \gg L_{c,z}$ in (17) and applied the expectation value over the y-surface-roughness in (22). If only a very small surface, for whose area A the condition $A \gg L_{c,y}L_{c,z}$ is not fulfilled, is scattering, the above loss coefficient stands for the ensemble average w.r.t. G, and higher order moments can be computed analogously. In typical applications, however, this condition is fulfilled and the loss coefficient will have a narrow distribution over G.

In general, the above calculations are valid within the explained approximations as long as the mode's fields can be simulated accurately. Hence, limitations on structural parameters, which previously arose due to approximations necessary for the calculation [10] or simulation [12], are eliminated by the semi-analytic approach and shifted to the mode simulation. For common integrated photonic applications, this enables the investigation of arbitrary waveguide geometries. For large, multimode platforms the scattering into the other modes also becomes significant and contributes to the propagation loss for the investigated mode, which is neglected in the above calculations.

So far, only a single sidewall was considered, but accounting for multiple surfaces is straightforward. It stands to reason that the Gaussian processes of the individual surfaces are uncorrelated [10], and thus, the calculated loss coefficients may be added for typical fabrication conditions.

III. Comparison to Established Models

In this section, the outlined calculation of the surface-roughness-induced scattering loss coefficients is conducted and evaluated vs. propagation loss measurements of photonic integrated circuits (PICs). We include comparisons to previous theoretical models from Payne and Lacey [7], Yap et al. [13], Poulton et al. [11], and Barwicz and Haus [10]. As mentioned above, the statistical properties along the waveguide length and height have a significant impact on the scattering loss. To the best of our knowledge, previous publications that include the measurements of the propagation loss and the surface roughness only evaluated the latter along the waveguide length. Hence, we infer the value of $L_{c,y}$ for which our model agrees. We simulate the waveguide system in Ansys Lumerical (version: 2022 R1, module: MODE, solver: Finite Difference Eigenmode (FDE)).

The comparison of the models is summarized in Table I, and the detailed analysis is described in the following:

TABLE I
COMPARISON OF PREDICTED SIDEWALL-ROUGHNESS-INDUCED SCATTERING LOSSES TO MEASURED PROPAGATION LOSS IN VARIOUS PUBLICATIONS

Ref.	Type	Width x height in nm	Wavelength in nm	Mode	σ in nm	$L_{c,z}$ in nm	$L_{c,y}$ in nm	Measured propagation loss in dB cm^{-1}	Scattering Loss by our model in dB cm^{-1}
[28]	Si strip, SiO_2 cladding	440 x 220	1550	TE	1	20	220	0.40 ± 0.06	0.40
[29]	Si strip, air cladding	500 x 220	1550	TE	0.95 ± 0.17	36 ± 12	∞	1.87 ± 0.49	1.73 ± 0.75
[11]	InPGaAs pedestal, air cladding	600 x 700	1550	TE	5 ± 1	56 ± 14	∞	70 ± 10	54 ± 23
[11]	InPGaAs pedestal, air cladding	600 x 700	1550	TM	5 ± 1	56 ± 14	∞	40 ± 10	7 ± 3
[13]	Si rib, SiO_2 cladding	1000 x 1800	1530 to 1560	TE	7.7 ± 1.0	160 ± 25	∞	6.8 ± 1.2	6.3 ± 3.2
[13]	Si rib, SiO_2 cladding	1000 x 1800	1530 to 1560	TM	7.7 ± 1.0	160 ± 25	∞	6.6 ± 2.6	4.6 ± 2.2
[13]	Si rib, SiO_2 cladding	1000 x 1800	1530 to 1560	TE	3.6 ± 0.2	225 ± 30	∞	0.8 ± 0.5	0.73 ± 0.17
[13]	Si rib, SiO_2 cladding	1000 x 1800	1530 to 1560	TM	3.6 ± 0.2	225 ± 30	∞	0.5 ± 0.3	0.52 ± 0.12

Horikawa et al. [28] fabricated silicon on insulator (SOI) strip waveguides with ArF immersion lithography. The strip waveguide had a height of 220 nm and a width of 440 nm, and was clad with a SiO_2 cladding. The refractive indices were determined with ellipsometry at a wavelength of 1550 nm to 3.48 for the Si core and 1.44 for the cladding. The surface roughness was evaluated via the edge pattern observed with scanning electron microscopy (SEM) and an exponential autocorrelation function was fitted with $\sigma = 1$ nm and $L_{c,z} = 20$ nm. The propagation loss was measured for dedicated test structures of varying lengths. They were designed for the fundamental TE-like mode at a wavelength of 1550 nm. Eventually, the propagation loss is estimated to (0.40 ± 0.06) dB cm^{-1}. They compared this experimental value to predictions by the theoretical model from Payne and Lacey [7], which predicts 0.7 dB cm^{-1}. The model from Barwicz and Haus [10] underestimates and results in 0.28 dB cm^{-1}. Finally, our model agrees exactly for $L_{c,y} = H = 220$ nm with a predicted value of 0.40 dB cm^{-1}. However, we obtain a large possible range from 0.09 dB cm^{-1} to 0.54 dB cm^{-1} for $L_{c,y} = 20$ nm and ∞, respectively. Evidently, $L_{c,y}$ has a significant impact and even a moderate deviation from perfect vertical striations ($L_{c,y} = \infty$) is important.

Fursenko et al. [29] manufactured Si nanowire waveguides on a SOI platform without a cladding. They had a height of 220 nm and a width of 500 nm. They were operated at a wavelength of 1550 nm in the TE-like mode. The core and substrate had a refractive index of 3.474 and 1.44, respectively. They used two processes with different etch chemistry: CF_4/Cl_2 and Cl_2. We analyze the latter, since with that they present four data points and we are able to get a statistical estimate. Further, we use the AFM data of the sidewall roughness, since Fursenko et al. argue that it is more consistent. They measured a propagation loss of (1.87 ± 0.49) dB cm^{-1}, a roughness RMS of $\sigma = (0.95 \pm 0.17)$ nm and correlation length of $L_{c,z} = (36 \pm 12)$ nm. They applied the Payne and Lacey model and obtained a prediction for the sidewall roughness induced scattering loss of (0.46 ± 0.20) dB cm^{-1}. Our model predicts (1.73 ± 0.75) dB cm^{-1} for $L_{c,y} = \infty$ and (1.28 ± 0.56) dB cm^{-1} for $L_{c,y} = 220$ nm. We observe, that the former estimate fits the measured propagation losses better, but the uncertainty of both propagation loss and surface roughness data is too high to make a definitive judgment.

Poulton et al. [11] structured a pedestal waveguide for a wavelength of 1550 nm. The structure had a width of 600 nm and was on top of an InP substrate. The InPGaAs core had a height of 700 nm, and a refractive index of 3.42. The pedestal was of InP with a height of 1500 nm, and a refractive index of 3.17. The waveguide had a cap of the same material with a height of 300 nm. The refractive index values were taken from Fujii et al. [30]. On the sides of the pedestal was air. Poulton et al. measured the surface roughness with an AFM and obtained a RMS $\sigma = (5 \pm 1)$ nm and a correlation length of $L_{c,z} = (56 \pm 14)$ nm. They measured a propagation loss of (7 ± 1) dB mm^{-1} for the TE-like mode and (4 ± 1) dB mm^{-1} for the TM-like mode. They utilize their coupled mode theory to construct the radiation modes and obtain a prediction of (5.7 ± 4.4) dB mm^{-1} and (1.5 ± 1.2) dB mm^{-1}. They also evaluate a modified Payne and Lacey method [31], which estimates (0.53 ± 0.45) dB mm^{-1} and (0.20 ± 0.17) dB mm^{-1}. Applying our model, we are able to consider the surface roughness over the whole side of the waveguide, not just the core. We find the best fit for vertical striations with $L_{c,y} = \infty$, which results in (5.4 ± 2.3) dB mm^{-1} and (0.7 ± 0.3) dB mm^{-1}. Hence, the predicted scattering loss for the TE-like mode does not quite agree with the measured propagation loss, but it agrees with the coupled mode theory within the uncertainty and is a significant improvement to the Payne and Lacey model. The prediction for the TM-like mode falls short of the measured propagation loss, as do the other models. Poulton et al. argued, that additional material or leakage losses might bring the predicted values closer to the observed propagation losses. Moreover, if the top or bottom surface roughness is comparable to the sidewall roughness, it would also contribute, especially for the TM-like mode. As the authors mention, the high uncertainty bounds of the predictions necessitate a more precise measurement of the surface roughness parameters.

Yap et al. [13] fabricated rib waveguides on a (100) p-type SOI wafer which had a 2.5 μm Si layer on a buried 0.4 μm SiO_2 and covered them with a 0.5 μm SiO_2 layer. They targeted an etch depth of 1.8 μm and utilized fabrication processes differing mainly by their pattern transfer techniques and resist chemistries. They structured multiple widths and related the excess propagation loss to the 2 μm wide waveguides. They measured with a broadband light source covering the wavelength range from 1530 nm to 1560 nm. The surface roughness parameters were obtained by analyzing the line edge pattern in SEM images. They evaluated the excess loss of thinner waveguides w.r.t. the 2 μm wide one. We reproduced the propagation loss for the contact lithography and the E-beam lithography with negative resist with our model. The parameters and losses are listed in Table I. Because Yap et al. treated the excess loss, we simulate

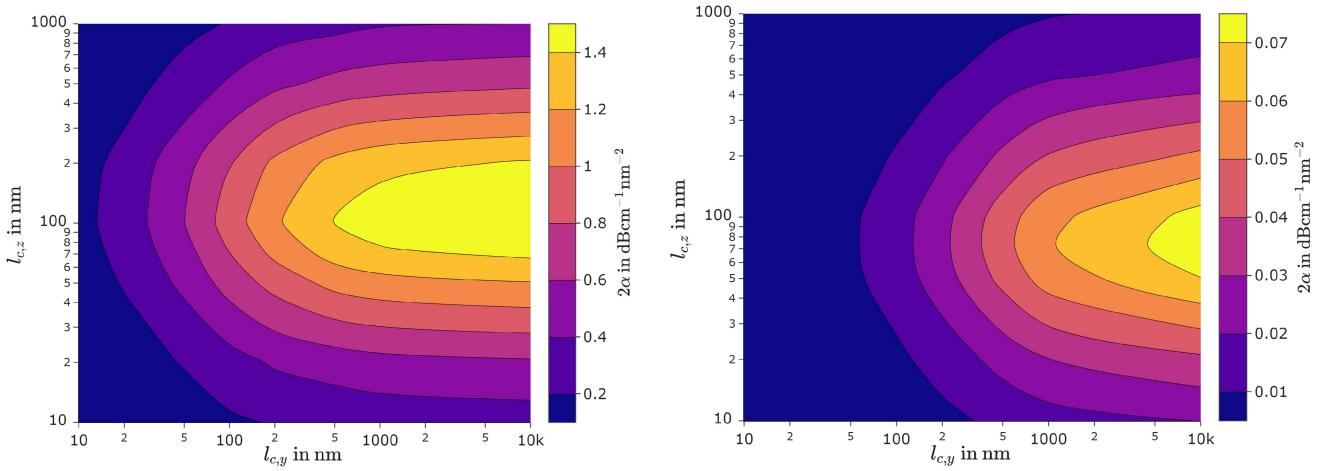

(a) TE-like, $440\,\mathrm{nm} \times 220\,\mathrm{nm}$ Si strip with SiO_2 cladding [28]

(b) TM-like, $1000\,\mathrm{nm} \times 1800\,\mathrm{nm}$ Si rib with SiO_2 cladding [13]

Fig. 2. Predicted loss coefficient 2α over the correlation lengths $L_{c,y}, L_{c,z}$ for the surface-roughness-induced scattering, normalized by σ^2.

the 1 μm and 2 μm ribs, and refer the loss of the former to the latter. We fixed the wavelength to 1550 nm and assumed refractive indices of 3.48 for the Si and 1.45 for the SiO_2, since they are not listed. We also evaluated multiple other wavelengths within the above range but observed only a marginal impact. We find that the predicted values agree with the measured ones within the uncertainty. Again we observe that vertical striations with $L_{c,y} = \infty$ result in the best match. Once more, the model shows a huge dependency on $L_{c,y}$. Yap et al. also modified the Payne and Lacey model with a factor that aims to correct for the electric field overlap with the sidewalls. However, it consistently underestimated the measured losses and our model is again more accurate.

IV. Discussion

The added complexity due to the two-dimensional kernel from (7) leads to difficulties due to arbitrariness in evaluating the presented surface-roughness-induced scattering model based on published data. It was shown above that the previously neglected correlation length along the waveguide height has a significant impact on the loss coefficient and an increase with larger values was observed. In Fig. 2 the behavior of the sidewall-roughness-induced scattering over both correlation lengths for an exponential kernel is substantiated. In Fig. 2(a) the system presented by Horikawa et al. [28] is analyzed. Indeed, we notice that our model predicts a monotonous increase with $L_{c,y}$, and an eventual saturation. By contrast, w.r.t. $L_{c,z}$ the situation is different and we observe a clear maximum. In comparison, the scattering of the TM-like mode in the Si rib waveguide system fabricated by Yap et al. [13] is shown in Fig. 2(b). We recognize that even though the mode and geometry are quite different, the result is qualitatively similar. However, the maximum is shifted to slightly lower values of $L_{c,z}$, and the saturation to higher values of $L_{c,y}$.

The contrasting characteristics w.r.t. the two correlation lengths can be explained by the special role that is attributed to the z-direction as the modes' propagation axis (2). Accordingly, the mode profile $\boldsymbol{e}(x, y)$ and each scattering current source are in phase in a given x, y-plane. Thus, a lower $L_{c,y}$ leads to less coherence within this cross section. By contrast, the mode oscillates in z with the wavelength $\lambda = \lambda_0/n_e$. If this is equal to the mean length in which the Gaussian process has one zero-level upcrossing, the surface roughness follows the mode oscillation and maximum coherence of the scattered radiation is established. According to Rasmussen and Williams [24], this characteristic length is equal to $2\pi L_{c,z}$. Hence, equality is established for $L_{c,z} = \frac{\lambda}{2\pi} = \beta^{-1}$. For the modes in the systems from Horikawa et al. [28] and Yap et al. [13], we receive the critical correlation lengths 106 nm and 73 nm, respectively. Evidently, these values correspond accurately to the maxima in Fig. 2(a) and (b), respectively. In summary, maximum scattering is caused when its sources have high coherence in the cross section and oscillate in unison with the mode in the z-direction, thus mimicking the behavior of the mode from the definition in (2).

V. Conclusion

We developed an ab initio, semi-analytical model for the surface-roughness-induced scattering loss in guided-wave systems. It incorporates the surface roughness as a perturbation in the permittivity in the manner of the volume current method [10]. Utilizing the adapted form of Johnson et al. [18], we found a closed-form solution for the loss coefficient of arbitrary refractive index profiles, including systems with high index contrast. By extension, our model is flexible concerning wavelength, materials, fabrication process, geometry, and mode, as it may be readily adapted to any waveguide or fiber system as long as the parameters of the roughness introduced by the fabrication processes are known. The mode of consideration is incorporated via its electromagnetic field amplitudes, which can be simulated using an electrodynamics software suite. In contrast to other approaches [10], [12], [17], no additional assumptions are needed and it may be integrated seamlessly into design software

for integrated photonics to provide an in-situ prediction of the scattering losses.

We considered the surface roughness as a Gaussian process via its autocorrelation function (7), which allows the fully coherent calculation and also takes the correlation along the waveguide height into account. In the past, it was mostly assumed that the sidewall roughness can be viewed as perfect vertical striations [9], [10], [11], [12], [14]. However, deviations of varying magnitude can be found in published AFM measurements [11], [19], [20], [21] and in a previous anisotropy analysis [16]. Using other models, it is challenging to deviate from this simplification. Moreover, previous roughness measurements only evaluate the correlation length along the waveguide length and neglect the perpendicular part. However, as our above calculations demonstrate, the exact form of the surface roughness' correlation has a significant impact on the scattering behavior (see Fig. 2). These observations give a clear indication of how different fabrication processes relate w.r.t. the surface-roughness-induced scattering. Accordingly, a reduction in $L_{c,y}$ always leads to better performance, whereas this is not the case for $L_{c,z}$.

For the analyzed data, we also find that an anisotropic kernel with a large correlation length in the height fits best, but a definitive quantification can only be stated case-wise for a specific fabrication process. Furthermore, in a recent publication we analyzed various kernels for their descriptive power of an example fabrication process [32]. We observed that kernels of the Matérn class fit the statistics better than the commonly applied exponential and squared-exponential kernels. Based on the above observations, a modified correlation function is expected to further affect the scattering coefficient. Hence, more thorough, holistic statistical evaluations of the surface roughness are necessary.

We compared our model to propagation loss measurements for a wide range of waveguide systems in Table I. Further, we checked its accuracy in comparison to other approaches, including the Payne and Lacey model [7], the variation presented by Yap et al. [13], coupled mode theory described by Poulton et al. [11], and the volume current method by Barwicz and Haus [10]. We consistently observed a better performance compared to the Payne and Lacey, and Barwicz and Haus models, and similar predictions to the coupled mode theory. After validation on a more extensive dataset regarding the surface roughness, we believe that our model is a useful addition to existing ones for the design of integrated optic systems.

ACKNOWLEDGMENT

The authors would like to thank Alexander Schossmann for the involved yet fruitful discussions about optical scattering. Furthermore, the authors would also like to thank Anton Buchberger for his tremendous help with the simulations.

REFERENCES

[1] L. Chrostowski and M. Hochberg, *Silicon Photon. Design*. Cambridge, U.K.: Cambridge Univ. Press, 2015. [Online]. Available: https://www.cambridge.org/core/books/silicon-photonics-design/BF3CF13E8542BCE67FD2BBC7104ECEAB

[2] E. Luan, H. Shoman, D. M. Ratner, K. C. Cheung, and L. Chrostowski, "Silicon photonic biosensors using label-free detection," *Sensors*, vol. 18, no. 10, 2018, Art. no. 3519.

[3] D. J. Blumenthal, R. Heideman, D. Geuzebroek, A. Leinse, and C. Roeloffzen, "Silicon nitride in silicon photonics," *Proc. IEEE*, vol. 106, no. 12, pp. 2209–2231, Dec. 2018.

[4] P. Steglich et al., "Silicon photonic micro-ring resonators for chemical and biological sensing: A tutorial," *IEEE Sensors J.*, vol. 22, no. 11, pp. 10089–10105, Jun. 2022.

[5] W. Bogaerts et al., "Silicon microring resonators," *Laser Photon. Rev.*, vol. 6, pp. 47–73, 2012. [Online]. Available: https://onlinelibrary.wiley.com/doi/10.1002/lpor.201100017

[6] B. Zhang et al., "Compact multi-million Q resonators and 100 mHz passband filter bank in a thick-soi photonics platform," *Opt. Lett.*, vol. 45, pp. 3005–3008, 2020.

[7] F. P. Payne and J. P. Lacey, "A theoretical analysis of scattering loss from planar optical waveguides," *Opt. Quantum Electron.*, vol. 26, no. 10, pp. 977–986, 1994. [Online]. Available: https://link.springer.com/article/10.1007/BF00708339

[8] S. G. Johnson, M. L. Povinelli, M. Soljačić, A. Karalis, S. Jacobs, and J. D. Joannopoulos, "Roughness losses and volume-current methods in photonic-crystal waveguides," *Appl. Phys. B*, vol. 81, no. 2, pp. 283–293, 2005. [Online]. Available: https://link.springer.com/article/10.1007/s00340-005-1823-4

[9] A. Melloni, D. Melati, and F. Morichetti, "Real photonic waveguides: Guiding light through imperfections," *Adv. Opt. Photon.*, vol. 6, no. 2, pp. 156–224, 2014. [Online]. Available: https://www.osapublishing.org/viewmedia.cfm?uri=aop-6-2-156

[10] T. Barwicz and H. Haus, "Three-dimensional analysis of scattering losses due to sidewall roughness in microphotonic waveguides," *J. Lightw. Technol.*, vol. 23, no. 9, pp. 2719–2732, Sep. 2005. [Online]. Available: https://ieeexplore.ieee.org/document/1506850/

[11] C. G. Poulton et al., "Radiation modes and roughness loss in high index-contrast waveguides," *IEEE J. Sel. Topics Quantum Electron.*, vol. 12, no. 6, pp. 1306–1320, Nov./Dec. 2006.

[12] C. Ciminelli, F. Dell'Olio, V. M. Passaro, and M. N. Armenise, "Fully three-dimensional accurate modeling of scattering loss in optical waveguides," *Opt. Quantum Electron.*, vol. 41, no. 4, pp. 285–298, 2009. [Online]. Available: https://link.springer.com/article/10.1007/s11082-009-9343-9

[13] K. P. Yap et al., "Correlation of scattering loss, sidewall roughness and waveguide width in silicon-on-insulator (SOI) ridge waveguides," *J. Lightw. Technol.*, vol. 27, no. 18, pp. 3999–4008, Sep. 2009.

[14] S. Hughes, L. Ramunno, J. F. Young, and J. E. Sipe, "Extrinsic optical scattering loss in photonic crystal waveguides: Role of fabrication disorder and photon group velocity," *Phys. Rev. Lett.*, vol. 94, Jan. 2005, Art. no. 033903. [Online]. Available: https://journals.aps.org/prl/abstract/10.1103/PhysRevLett.94.033903

[15] S. A. Schulz, "Propagation loss in slow light photonic crystal waveguides," Ph.D. dissertation, School Phys. Astron., Univ. St. Andrews, St. Andrews, U.K. Jun. 2012. [Online]. Available: https://research-repository.st-andrews.ac.uk/handle/10023/2837

[16] E. Jaberansary, T. M. Masaud, M. M. Milosevic, M. Nedeljkovic, G. Z. Mashanovich, and H. M. Chong, "Scattering loss estimation using 2-D fourier analysis and modeling of sidewall roughness on optical waveguides," *IEEE Photon. J.*, vol. 5, no. 3, 2013, Art. no. 6601010.

[17] D. M. Kita, J. Michon, S. G. Johnson, and J. Hu, "Are slot and subwavelength grating waveguides better than strip waveguides for sensing?," *Optica*, vol. 5, no. 9, pp. 1046–1054, 2018. [Online]. Available: https://arxiv.org/abs/1805.03321http://dx.doi.org/10.1364/OPTICA.5.001046

[18] S. G. Johnson, M. Ibanescu, M. A. Skorobogatiy, O. Weisberg, J. D. Joannopoulos, and Y. Fink, "Perturbation theory for Maxwell's equations with shifting material boundaries," *Phys. Rev. E*, vol. 65, Jun. 2002, Art. no. 066611. [Online]. Available: https://journals.aps.org/pre/abstract/10.1103/PhysRevE.65.066611

[19] J. H. Jang et al., "Direct measurement of nanoscale sidewall roughness of optical waveguides using an atomic force microscope," *Appl. Phys. Lett.*, vol. 83, pp. 4116–4118, 2003. [Online]. Available: https://aip.scitation.org/doi/10.1063/1.1627480

[20] S. Roberts, X. Ji, J. Cardenas, M. Corato-Zanarella, and M. Lipson, "Measurements and modeling of atomic-scale sidewall roughness and losses in integrated photonic devices," *Adv. Opt. Mater.*, vol. 10, no. 18, 2022, Art. no. 2102073. [Online]. Available: https://onlinelibrary.wiley.com/doi/10.1002/adom.202102073

[21] G. Pandraud, E. Margallo-Balbas, C.-K. Yang, and P. J. French, "Experimental characterization of roughness induced scattering losses in PECVD SiC waveguides," *J. Lightw. Technol.*, vol. 29, no. 5, pp. 744–749, 2011. [Online]. Available: https://ieeexplore.ieee.org/document/5701637/

[22] S. G. Johnson, P. Bienstman, M. A. Skorobogatiy, M. Ibanescu, E. Lidorikis, and J. D. Joannopoulos, "Adiabatic theorem and continuous coupled-mode theory for efficient taper transitions in photonic crystals," *Phys. Rev. E. - Stat. Phys., Plasmas, Fluids, Related Interdiscipl. Topics*, vol. 66, Dec. 2002, Art. no. 066608.

[23] M. Skorobogatiy, S. G. Johnson, S. A. Jacobs, and Y. Fink, "Dielectric profile variations in high-index-contrast waveguides, coupled mode theory, and perturbation expansions," *Phys. Rev. E. - Stat. Phys., Plasmas, Fluids, Related Interdiscipl. Topics*, vol. 67, 2003, Art. no. 046613.

[24] C. E. Rasmussen and C. K. I. Williams, *Gaussian Processes for Machine Learning*. Cambridge, MA, USA: MIT Press, 2005. [Online]. Available: https://direct.mit.edu/books/book/2320/gaussian-processes-for-machine-learning

[25] S. J. Orfanidis, "Electromagnetic waves and antennas," 2016. [Online]. Available: www.ece.rutgers.edu/orfanidi/ewa

[26] C. Chatfield and H. Xing, *The Analysis of Time Series*. London, U.K.: Chapman & Hall/CRC, 2019. [Online]. Available: https://www.taylorfrancis.com/books/9781498795647

[27] C.-L. Chen, *Foundations for Guided-Wave Optics*. Hoboken, NJ, USA: Wiley, 2006. [Online]. Available: https://onlinelibrary.wiley.com/doi/book/10.1002/0470042222

[28] T. Horikawa, D. Shimura, and T. Mogami, "Low-loss silicon wire waveguides for optical integrated circuits," *MRS Commun.*, vol. 6, pp. 9–15, 2016. [Online]. Available: https://link.springer.com/10.1557/mrc.2015.84

[29] O. Fursenko, J. Bauer, A. Knopf, S. Marschmeyer, L. Zimmermann, and G. Winzer, "Characterization of Si nanowaveguide line edge roughness and its effect on light transmission," *Mater. Sci. Eng.: B*, vol. 177, pp. 750–755, 2012.

[30] M. Fujii, C. Koos, C. Poulton, J. Leuthold, and W. Freude, "Nonlinear FDTD analysis and experimental verification of four-wave mixing in InGaAsP-InP racetrack microresonators," *IEEE Photon. Technol. Lett.*, vol. 18, no. 2, pp. 361–363, Jan. 2006.

[31] K. K. Lee, D. R. Lim, H.-C. Luan, A. Agarwal, J. Foresi, and L. C. Kimerling, "Effect of size and roughness on light transmission in a Si/Sio2 waveguide: Experiments and model," *Appl. Phys. Lett.*, vol. 77, pp. 1617–1619, 2000. [Online]. Available: https://aip.scitation.org/doi/10.1063/1.1308532

[32] S. Hörmann, J. W. Hinum-Wagner, J. Sattelkow, D. Rist, and A. Bergmann, "Comparison of gaussian process kernels for surface roughness modelling," in *Proc. 23rd Eur. Conf. Integr. Opt.*, 2022, pp. 57–59.